RL-TR-97-116
Final Technical Report
October 1997

# HIGH LINEARITY MODULATION IN QUANTUM WELLS FOR ANALOG FIBER OPTIC LINKS

University of California, San Diego

Sponsored by
Advanced Research Projects Agency
ARPA Order No. A233

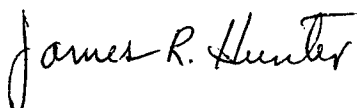*APPROVED FOR PUBLIC RELEASE; DISTRIBUTION UNLIMITED.*

19980113 036

The views and conclusions contained in this document are those of the authors and should not be interpreted as necessarily representing the official policies, either expressed or implied, of the Advanced Research Projects Agency or the U.S. Government.
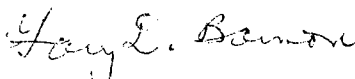
**Rome Laboratory
Air Force Materiel Command
Rome, New York**

DTIC QUALITY INSPECTED 3

This report has been reviewed by the Rome Laboratory Public Affairs Office (PA) and is releasable to the National Technical Information Service (NTIS). At NTIS it will be releasable to the general public, including foreign nations.

RL-TR-97-116 has been reviewed and is approved for publication.

APPROVED: *James R. Hunter*

JAMES R. HUNTER
Project Engineer

FOR THE DIRECTOR: *Gary L. Barmore*

GARY D. BARMORE, Major, USAF
Deputy Director, Surveillance & Photonics Directorate

# HIGH LINEARITY MODULATION IN QUANTUM WELLS
# FOR ANALOG FIBER OPTIC LINKS

Paul K. L. Yu
A. L. Kellner
Robert B. Welstand

| 1. AGENCY USE ONLY *(Leave blank)* | 2. REPORT DATE | 3. REPORT TYPE AND DATES COVERED | |
|---|---|---|---|
| | October 1997 | Final | Aug 93 - Feb 97 |

| 4. TITLE AND SUBTITLE | 5. FUNDING NUMBERS |
|---|---|
| HIGH LINEARITY MODULATION IN QUANTUM WELLS FOR ANALOG FIBER OPTIC LINKS | C  - F30602-93-C-0165 |
| **6. AUTHOR(S)** | PE - 61101E |
| | PR - A233 |
| Paul K. L. Yu, A. L. Kellner, and Robert B. Welstand | TA - 00 |
| | WU - 01 |

| 7. PERFORMING ORGANIZATION NAME(S) AND ADDRESS(ES) | 8. PERFORMING ORGANIZATION REPORT NUMBER |
|---|---|
| University of California, San Diego<br>Dept of Electrical & Computer Engineering<br>La Jolla, CA 92093-0407 | N/A |

| 9. SPONSORING/MONITORING AGENCY NAME(S) AND ADDRESS(ES) | 10. SPONSORING/MONITORING AGENCY REPORT NUMBER |
|---|---|
| Advanced Research Projects Agency   Rome Laboratory/OCPC<br>3701 North Fairfax Drive   25 Electronic Pky<br>Arlington, VA 22203-1714   Rome, NY 13441-4514 | RL-TR-97-116 |

**11. SUPPLEMENTARY NOTES**

Rome Laboratory Project Engineer:  J. R. Hunter/OCPC/(315) 330-7045
ARPA Project Manager:  B. M. Hendrickson/STO/(703) 516-7425

| 12a. DISTRIBUTION AVAILABILITY STATEMENT | 12b. DISTRIBUTION CODE |
|---|---|
| Approved for public release; distribution unlimited. | |

**13. ABSTRACT** *(Maximum 200 words)*

For many RF photonic applications, low RF insertion loss, large spurious free dynamic range (SFDR) links are needed.  This development program demonstrated a high saturation power (46 mW), high RF efficiency (-17.8 dB) analog semiconductor waveguide modulator based upon Franz-Keldysh Effect (FKE) modulation.  This was achieved with 43 mW optical power incident to the modulator.  The modulator was operated with a multi-octave SFDR of 106 dB-Hz (2/3), and a single octave SFDR of 124 dB-Hz (4/5).  Also introduced is a novel, dual function operation concept for the semiconductor electroabsorption modulator for operating also as an effective photodetector.  The photodetector can handle more than 20 mA of photocurrent.  The behavior of a waveguide modulator based upon FKE and Quantum Confined Stark Effect to achieve high linearity modulation was also modeled and documented.  A first time demonstration of high quality, strain compensated multiple quantum well InGaP/InAsP materials was accomplished.  Up to one micrometer thick strained multiple quantum well regions can be grown without degradation in the optical properties of the materials.

| 14. SUBJECT TERMS | | | 15. NUMBER OF PAGES |
|---|---|---|---|
| Multiple Quantum Well (MQW) devices; Franz-Keldysh devices; Optical Modulator; Dual Function transceiver | | | 52 |
| | | | 16. PRICE CODE |

| 17. SECURITY CLASSIFICATION OF REPORT | 18. SECURITY CLASSIFICATION OF THIS PAGE | 19. SECURITY CLASSIFICATION OF ABSTRACT | 20. LIMITATION OF ABSTRACT |
|---|---|---|---|
| UNCLASSIFIED | UNCLASSIFIED | UNCLASSIFIED | UL |

# High Linearity Modulation in Quantum Wells for Analog Fiber Optic Links

## Contents

## Acknowledgments

# 1. Executive Summary

In this program, we have achieved the following accomplishments.

We have demonstrated a high power, high RF efficiency (-17.8 dB) analog semiconductor waveguide modulator based upon Franz-Keldysh Effect (FKE) modulation at 1.3 μm wavelength. This is achieved with up to 43 mW optical power incident on the modulator. The modulator has been operated with a multi-octave spurious free dynamic range (SFDR) of 106 dB-Hz $^{2/3}$, and a single octave SFDR of 124 dB-Hz$^{4/5}$. These results have been found to be independent of frequency, up to 4 GHz. The highest frequency of operation of the modulator is beyond 30 GHz, while the packaged devices are tested up to 13.6 GHz.

In the course of this program, we have also studied and designed the waveguide modulator based upon a combination of FKE and Quantum confined Stark Effect (QCSE) for enhancing the link linear dynamic range. Preliminary modeling shows that a multi-octave SFDR of 120 dB-Hz$^{2/3}$ is possible for an optimized structure combining both effects.

We have designed and fabricated waveguide modulators based upon a longitudinal electric field modulation effect in quantum wells. The waveguide modulators based upon this effect showed optical modulation, however, the frequency of operation is presently limited by the lateral carrier transport in the intrinsic layer.

We have also demonstrated a dual function analog receive/transmit operation for the semiconductor electroabsorption modulator. We have demonstrated, by adjusting the bias voltage to the waveguide device, it can operate as an effective high saturation photodetector as well as an effective modulator. The waveguide photodetector can be operated with more than 20 mA of photocurrent and generated low harmonic signals.

We have also demonstrated under this program the first high quality strained compensated multiple quantum well InGaP/InAsP modulators at both 1.3 and 1.5 μm wavelength. Up to one micrometer thick multiple quantum well regions can be grown without degradation in the optical properties of the materials. These materials will be further studied for high power waveguide modulator designs.

2

## 2. Introduction and the overall technical objective

Optical transmission of analog RF signals has much potential for use in high-speed antenna remoting and RF distribution systems. Depending upon the bandwidth, dynamic range, noise figure, and cost requirements, one can choose systems that are based on either the direct modulation of a laser diode or the external modulation of laser using a waveguide modulator. External modulation is presently considered for the more demanding broadband RF link applications. However, two problems continue to affect the use of semiconductor waveguide modulators - the limited linear dynamic range and the large optical insertion loss. Improvement in these two areas would provide attractive alternatives for applications that could benefit from high-fidelity, analog optical links.

This program emphasized the study of semiconductor-based external modulators due to their potential advantages over other modulators for microwave transmission. The semiconductor modulators are small. The devices can be packaged at a higher density than, for example, lithium niobate based devices. The smaller size feature also allows the modulator to be treated as a lumped microwave capacitance, which will simplify the microwave electrode design. The ease of integrating semiconductor modulators with microwave electronics facilitates the assembly of the overall system, which can be important for many RF applications.

The overall objective of this program is to develop RF efficient, 1.3 $\mu$m wavelength, semiconductor waveguide modulator for high speed analog fiber-optic links. The use of organometallic vapor phase epitaxy for material synthesis is emphasized in this program as this epi-technology can facilitate large scale manufacturing of optoelectronic integrated circuits. Due to the optical loss and dispersion considerations in fibers, and the fact that high power lasers and optical amplifiers are available, materials for optical modulators in the 1.3 and 1.5 $\mu$m wavelengths have been considered. In particular, lattice matched InGaAsP/InP, bulk or quantum well materials, and strained InAsP/InP quantum well materials are investigated in this program. A main goal of this program is to design and experimentally demonstrate high speed waveguide modulators that can achieve low RF insertion loss and a two-tone, spurious-free dynamic range in excess of 100 dB in a one hertz bandwidth, and operate at high center frequency.

3

## 3. Waveguide modulator based on Franz-Keldysh Effect

The main issues of waveguide modulators, as mentioned above, are the RF insertion loss and the linear dynamic range that can be realized in a device with a single p-electrode design. In the past, the majority of studies on improving the linearity of optoelectronic modulators focused on the lithium niobate modulators. Recent work makes use of dual parallel modulation [1], mixed polarization [2], or other feedforward compensation schemes [3,4] that cause partial cancellation of the nonlinear components. Disadvantages for these feedforward approaches are the complexity of design and the tight tolerance requirements on the power splitters and recombining couplers.

Several approaches for enhancing linear dynamic range were studied in this program. This section will focus on the approach for enhancing linear dynamic range in through low-biasing the semiconductor electroabsorption modulator and through application of high optical power. The advantages of low bias are two-fold. First of all, the third-order intermodulation distortion is suppressed as the bias approaches a point on the transfer curve (light output versus bias voltage) that corresponds to a null for the third derivative. Secondly, the link gain increases when excess optical power is used to compensate the optical loss through low-biasing.

This approach was applied on a waveguide structure that employs an electroabsorbing InGaAsP layer, operating by the Franz-Keldysh effect (FKE) [5]. Except for slight modal disparity between the TE and TM polarizations in the waveguide, the FKE modulation mechanism is much less polarization sensitive [6,7] than other electrooptic effects. An additional feature of electroabsorption modulators is their small drive voltage.

The material for the waveguide modulator is synthesized by low pressure organometallic vapor phase epitaxy (OMVPE) in our laboratory. The growth temperature and the chamber pressure for OMVPE are set at $650^{\circ}C$ and 20 Torr respectively for achieving a high purity level for the intrinsic (InGaAsP) region of the device. In our MOVPE reactor, high purity sources such as trimethylindium, triethylgallium, arsine, phosphine are used for the group III and group V elements, while diethylzinc and silane are respectively used as p and n doping sources. The resulting layers are examined by X-

ray rocking curve analysis to compare the lattice constant of the epilayer (InGaAs) with that of the substrate. After epitaxy, Hall effect measurement and photoluminescence spectroscopy are used to examine the electronic and optical properties of the epilayers. Typically the residual doping concentration is on the order of $5 - 8 \times 10^{15}$ cm$^{-3}$, and is n-type (more details on growth are presented in Rome Lab report RL-TR-95-173).

The layer structure of the modulator is as follows: the active layer of the waveguide is a lattice-matched, 3500 Å thick, InGaAsP ($\lambda_Q$ = 1.24 µm) layer grown by OMVPE on n-type (S doped) InP substrate, sandwiched between p- and n-type InP layers, 1 µm and 0.375 µm thick, respectively (the thickness of the active layer has been selected based upon the link efficiency consideration). An additional p$^+$ InGaAs capping layer of 2000 Å is grown for ohmic contact. Rib-loaded waveguide structures have 5 µm mesa widths and are cleaved to 120 µm length. The waveguide facets are also anti-reflection coated and coupled to single mode fiber. The reverse breakdown voltage is in excess of 12 V. Typical 3 dB electrical bandwidth of the device measured for the link experiment is 11-13 GHz, with the highest exceeding 30 GHz, as measured from the device capacitance. A frequency measurement of a FKE waveguide modulator up to 20 GHz is shown in Fig. 1
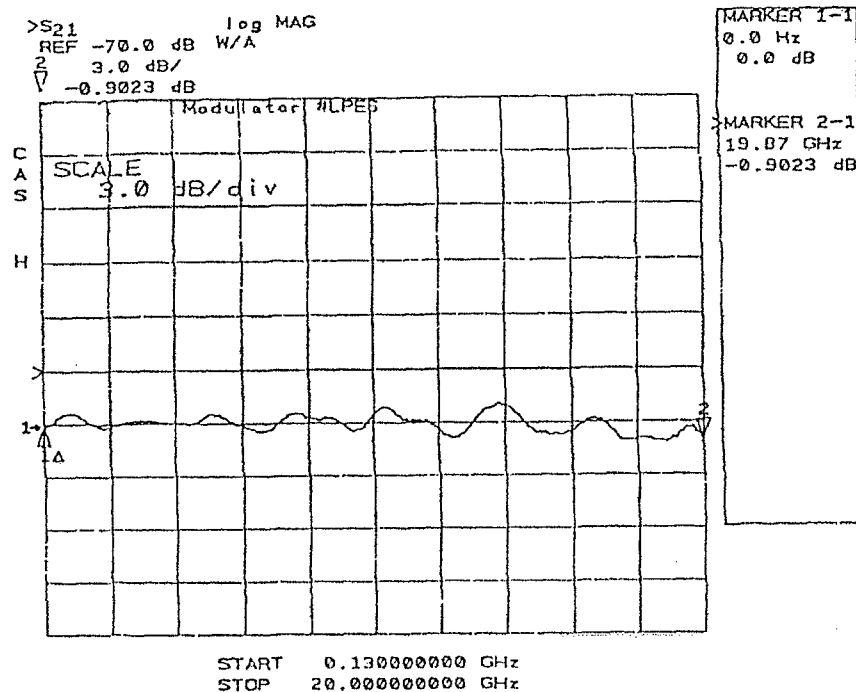


Fig. 1  The frequency response of an InGaAsP/InP FKE waveguide modulator at 1.32 µm wavelength.

### 3.1 Analog fiber link performance: modeling and experiment

It was demonstrated that large spurious free dynamic ranges (SFDR) can be obtained in a link with the FKE waveguide modulators by adjusting the DC bias. This is achieved by (a) low-biasing at the null in the (second) third derivative of the transfer curve for (multi-octave) single octave operation, (b) increasing the optical power to the modulator. However, only 3 dB of excess power is required to gain 22 dB in the dynamic range. This improvement is basically due to the exponential-like transfer function of the FKE modulator, for which the third-order derivative null is attained at a bias with a higher slope efficiency than that for the cosine-squared transfer function of the Mach-Zehnder.

Link measurements are performed over a range of DC bias conditions, RF power, RF frequencies and input polarization. The fundamental signal and the third-order distortion terms are investigated by two-tone testing at 4 GHz with 40 MHz tone separation. Similar two-tone results are obtained at 780 MHz and 1 GHz. The optical link consists of a Nd:YAG laser, a polarization controller, the modulator, and a Hewlett-Packard 70810B InGaAs receiver module and a spectrum analyzer. The input RF is supplied to the modulator from two HP 8630A signal generators through a power combiner and bias-T. Ferro-electric isolators are used to keep back-reflections from re-entering the RF sources.

A seventh-order polynomial is empirically fitted to the experimental DC transfer curve, and this transfer function is expanded in a McLaurin series about the different modulator bias voltages for determination of the distortion levels incident on the detector. The same method is used as in [8], but all terms up to $n = 5$ are included. For the third-order intermodulation power, we expect a fifth-order power dependence at the third-order null. Once the fundamental signal and distortion terms have been calculated as a function of modulation index, the SFDR is estimated for a given detector photocurrent and its corresponding noise floor.

### *Results at moderate optical power levels*

Characteristic static transfer curves at 1.32 μm wavelength for the TE and TM polarizations are shown in Figure 2a. There is a small, but distinct polarization

6

anisotropy apparent in these curves. This is due to different optical overlaps with the electroabsorbing layer for the TE and TM polarizations in the waveguide.

Figure 2b shows the simulated SFDR in a 1 Hz bandwidth, based on the TM transfer curve in Figure 2a, for a photocurrent of 2 mA. Both single octave and multi-octave SFDR are calculated. For single octave applications the SFDR is determined only by the odd-order intermodulation terms, as these occur very close in frequency to the signal frequencies. For multi-octave operation, all harmonics and all orders of intermodulation distortion must be considered to determine the SFDR. However, the second-order intermodulation is dominant for most applied biases.
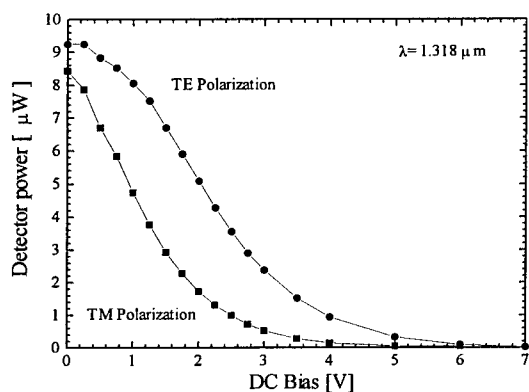


Fig. 2a. Direct current transfer curves for the TE and TM polarizations for a Franz-Keldysh waveguide modulator operated at 1.3 μm wavelength..
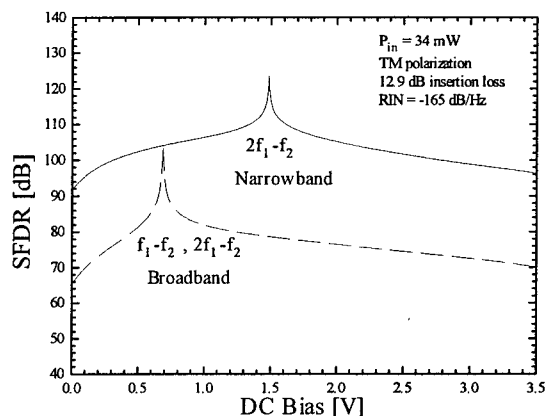
Fig. 2b. Simulated SFDR in a I-Hz bandwidth versus dc bias for the TM polarizations at 2 mA photocurrent. The upper curve shows SFDR for sub-octave applications, while the lower case is for the multi-octave applications.

The peak in the single octave SFDR near 1.5 V is noted. The simulation reveals that the third derivative of the transfer function crosses zero at this bias. Thus, the third-order term in the intermodulation distortion power drops out, and the fifth-order term dominates. With the distortion falling off at a fifth-order rate, the SFDR reaches 127 dB-$Hz^{4/5}$ at this bias. The peak itself is very narrow and this large dynamic range is only

possible with precise control of the DC bias. It should be noted that a SFDR greater than 120 dB in a 1 Hz bandwidth is attained with a voltage variation of less than 50 mV. Under multi-octave operation, the simulated SFDR curve also demonstrates a peak, occurring at 0.7 V bias. This is the bias at which the second derivative of the transfer function has a null, and the SFDR is then determined by the third-order intermodulation term. The simulation also projects a multi-octave SFDR of 104 dB-Hz$^{2/3}$ at the second order null, with 2 mA of photocurrent incident on the detector for the transfer curve of TM polarization shown in Fig. 2a.

The experimental results are plotted in Figures 3a and 3b for the TM polarization at low incident optical power levels. In Figure 3a, the detected RF signal and third-order intermodulation powers are plotted against the input RF power at the DC bias corresponding to the peak in the SFDR. The experiment shows the third-order intermodulation has a slope of 5 dB/dB at that bias. Adjusting the bias a few tenths of a volt above or below the peak, the slope becomes 3 dB/dB. Figure 3b shows the measured and simulated SFDR versus bias voltage for constant optical power at the modulator input. For an unmatched detector, a thermal-limited noise floor of -168 dBm is used in determining the SFDR. The single octave and multi-octave SFDR are 89.7 dB and 79 dB, respectively, in a 1 Hz bandwidth at detector photocurrents of 3.8 µA and 8.4 µA. One can project the SFDR for shot noise-limited detection at 2 mA, assuming that the RF signal and relative distortion terms scale linearly. This assumption is reasonable for these moderate power levels.
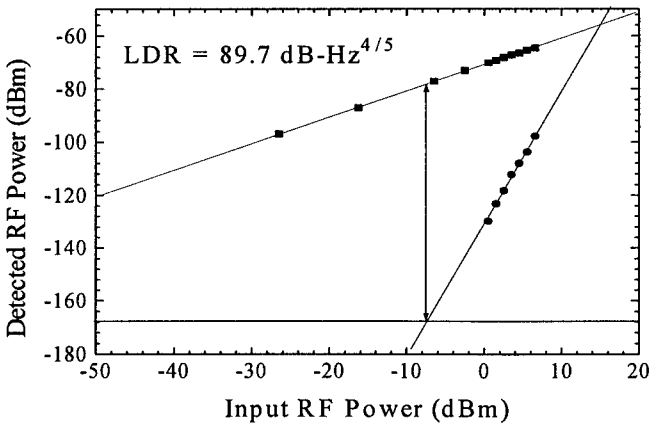
Fig. 3a. The detected RF signal and third-order intermodulation powers are shown versus the input RF power at the dc bias corresponding to the peak in the SFDR (at 3.8 µA detector photocurrent).
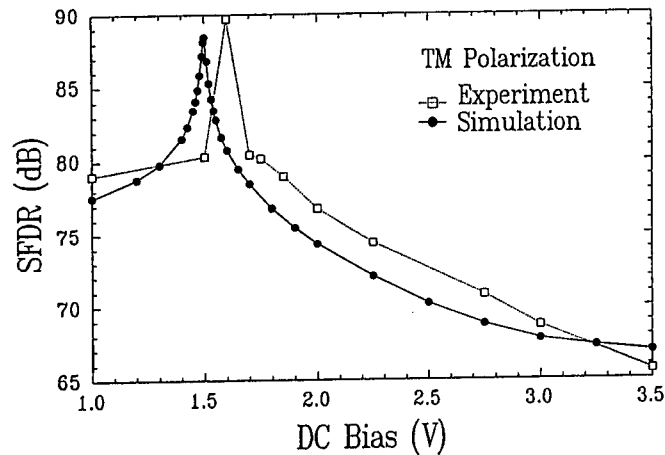
Fig. 3b. The measured and simulated SFDR in a 1-Hz bandwidth versus
dc bias for constant optical power at the modulator input.

The projected single octave and multi-octave SFDR are 129 dB-Hz$^{4/5}$ and 107 dB-Hz$^{2/3}$, respectively, which agree closely to the simulated results of 127 dB-Hz$^{4/5}$ and 104 dB-Hz$^{2/3}$. The experimental results at high power will be presented below.

The simulated link RF efficiency curves (based on Figure 2a transfer curves) for the TE and TM polarizations display some anisotropy. The efficiency for TM polarization attains its maximum of -61 dB at 0.75 V bias, and the efficiency for TE polarization attains its maximum of -64 dB at 2.0 V. The detector photo-currents for these simulated link gains are in the μA range. Due to the smaller switching voltage for the TM transfer curve, the RF efficiency falls off faster with increasing DC bias than for the TE polarization. Subsequently, there is a crossover at approximately 1.5 V, at which the RF efficiencies for the two polarizations both equal -65 dB. This crossover point has also been verified experimentally. As the polarization is rotated, the RF response is the same. At this bias, the modulator is effectively polarization insensitive. There is a tradeoff of 4 dB in RF efficiency as compared to the TM maximum at 0.75 V. However, an excess optical power of 2 dB can be added at the input of the modulator to compensate the equivalent power loss due to adjusting the bias. Therefore, low-biasing the FKE waveguide modulator can also give rise to polarization independent RF operation.

*Results at high power levels*

As noted above, the modulator can be operated with a large dynamic range and large RF efficiency. These are simultaneously maximized in broadband or multiple-

octave applications by biasing the waveguide device at the point on the DC transfer curve at which the second derivative is zero. To further enhance both parameters, optical power to the modulator is increased. Measurement was performed on a second device that has the null point at 2.0 V. The linearity is investigated for the modulator biased at 2.0 V, and the results of the two-tone measurements at 4.0 GHz are shown in Fig. 4a. The dominant distortion is the third-order intermodulation term. The third-order intercept point (IP3) is -3.6 dBm (output referenced), thus the multi-octave SFDR extrapolated to the noise floor is measured to be 106 dB for a 1 Hz noise bandwidth (Fig. 4a). This link dynamic range is a broadband result, which means the link is useful over the full bandwidth of the device.

As before, a reduction of third-order intermodulation terms can be achieved by biasing the modulator at the point on the transfer curve where the third derivative is zero. By biasing at the third-order null point, 3.8 V, with the same optical input power we measured a single octave SFDR of 124 dB in a 1 Hz noise bandwidth (Fig. 4b). The dominant intermodulation distortion is the fifth order provided the second and fourth order can be band-filtered.
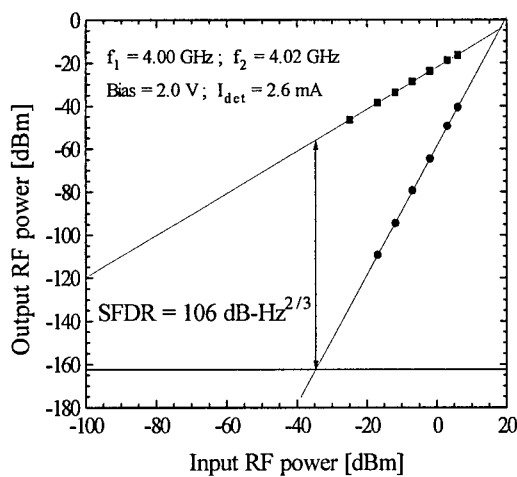


Fig. 4a. SFDR at high incident optical powers, for the multi-octave measurement, with 43 mW (TM polarized) light incident on the modulator, the SFDR at 4 GHz is 106 dB-Hz$^{2/3}$ with 2.6 mA of detector photocurrent.
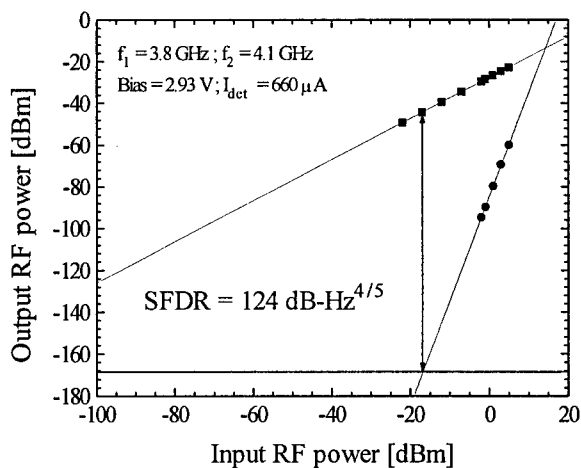
Fig. 4b. For the single octave measurement, with 37 mW light incident onto the device, the SFDR at 4 GHz is 124 dB-Hz$^{4/5}$ with 0.66 mA of photocurrent.

Fig. 5 shows the measured RF gain versus the input optical power for the modulator biased at 2.0 V, giving the largest RF gain possible for this device. The RF gain of the link shows no saturation up to 43 mW optical power, the largest power available for this measurement. The large power handling capability of the modulator enables a substantial RF signal gain, despite the small depths of modulation for spurious signal-free operation. The maximum measured link gain is -17.8 dB with 3.0 mA of DC photocurrent generated in the external detector.
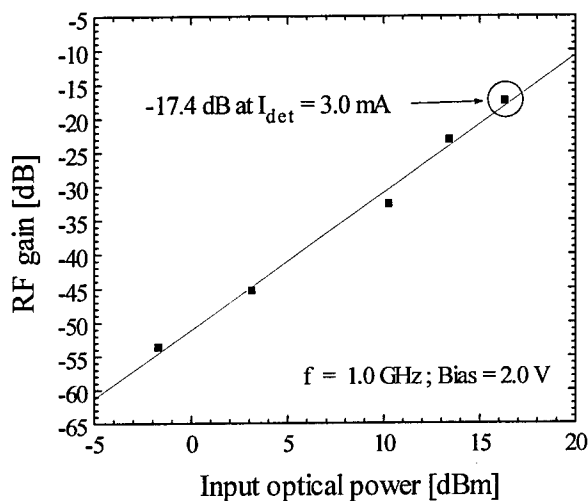


Fig. 5. RF gain at 1 GHz versus input optical power of the transceiver as a waveguide modulator.

## Main results of section 3

Low-biasing the FKE waveguide modulator is shown to increase the SFDR by 22 dB with only a 3 dB optical power penalty. Polarization independent RF operation is also obtained with bias adjustment.

At an incident optical power of 43 mW, the multi-octave spurious-free dynamic range of the modulator is 106 dB-Hz$^{2/3}$, which corresponds to an IP3 of -3.6 dBm. The highest RF link gain of the modulator is -17.8 dB. The single-octave spurious-free dynamic range of the modulator is 124 dB-Hz$^{4/5}$. SFDR and link gain measurements are performed at fundamental frequencies of 780 MHz, 1 GHz and 4GHz, and they indicated no frequency dependence except that of the Epitaxx detector used at the receiver.

11

## 4.    Modulator/detector operation of the electroabsorption device

Analog fiber optic (FO) links are useful in antenna remoting and active phased array applications for delivering high frequency RF signals directly to and from antenna elements with minimal signal attenuation, high dynamic range, and negligible element crosstalk.  As the microwave frequency of operation is increased above 10 GHz, phased array antenna element spacing becomes restrictively small resulting in severe front end space and EMI limitations.  Small, multiple-function optoelectronic transceiver components can be useful for mitigating these limitations. The system packaging size or form factor advantage is further emphasized if dual function modulator/detector operation can be obtained resulting in extremely compact transmit/receive front end antenna architectures.  The multifunction aspect of the semiconductor waveguide device is the subject of this section.

Giuliani, et al., [9] have recently demonstrated a multifunctional amplifier-modulator-detector for digital photonic networks.  This two-electrode device acts as a modulator and power amplifier or as a pre-amplifier and detector.  In this program, a single-electrode device transmitter and receiver (transceiver) for use in either single- or multi-element antenna remoting applications is demonstrated.  Fundamental for the operation of the transceiver is the Franz-Keldysh effect (FKE) described in the Section 3. This electroabsorption mechanism serves a dual-purpose:  (1) to apply modulation with moderate absorption, and (2) for photodetection at strong absorption. We have shown that efficient RF modulation and detection are obtainable in the same waveguide structure. To our knowledge, this is the first reported single-electrode waveguide device intended for use as both a modulator and a detector in an analog fiber optic link.

The transceiver only requires one optoelectronic device at the antenna front end. It must possess an adjustable DC electrical bias and a dual-band matching circuit, which may be integrated on-chip, at the remote site. Frequency conversion or other signal processing may be done remotely at the site of the laser source. This makes a very simple antenna front end architecture.  A schematic of the proposed transceiver is illustrated in Fig. 6.  The waveguide device works as a modulator in receive mode and a detector in transmit mode and can be switched by simultaneously adjusting the DC electrical bias

and activating the T/R switch. The modulation and detection characteristics of the semiconductor device are critical to this approach and results show that little link performance is sacrificed in comparison to using a dedicated optical modulator and detector.
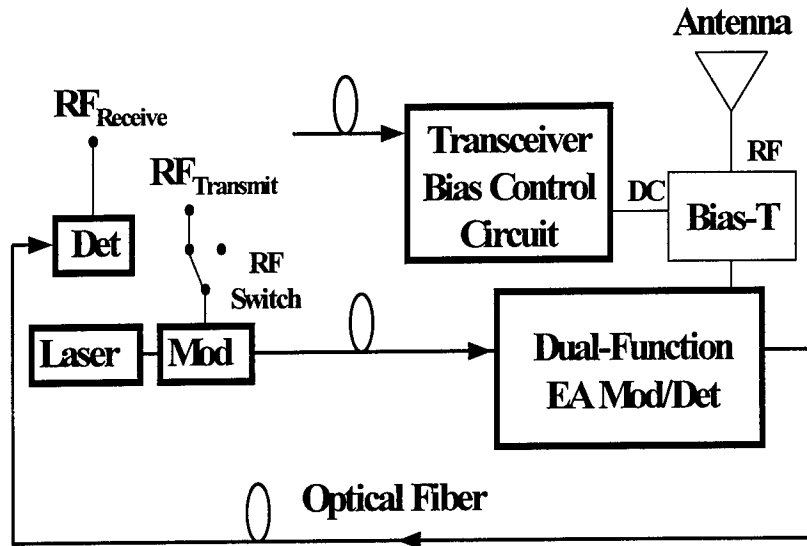


Fig. 6. Schematic of antenna feed network, including opto-electronic transceiver, remote laser, optical detector (Det), and modulator (Mod), used for transmit/ receiver applications.

The performance of the transceiver for use as a modulator is described in Section 3. The transceiver for use as a detector is biased at 7.0 V to assure large absorption. Saturation is investigated by varying the optical power incident to the detector. Fig. 7 shows the detected RF signal power plotted versus input optical power. The measurement shows no saturation for power levels up to 4.0 mW, and the measured RF power agrees with values calculated from the measured DC responsivity, $\mathcal{R}$, of 0.47 mA/mW.

In the heterodyned configuration with 100% modulation depth, the RF gain is given by $P_{OPT} \bullet \mathcal{R}^2 \bullet R_d$, where $R_d$ is the load impedance (50 $\Omega$) and $P_{OPT}$ is the optical power. The transceiver RF gain is thus +16 dB. Using a conventional InGaAs detector gives a larger RF gain, e.g. +20.7 dB for a responsivity of 0.77 mA/mW. Therefore, the smaller responsivity of the waveguide detector results in a theoretical noise figure penalty

13

of 4.7 dB compared to the conventional InGaAs detector. Measurements show, at the same optical power level, a difference in RF signal of -3.3 dB at 4.0 GHz between the transceiver and the conventional detector. The discrepancy is explained as the Epitaxx InGaAs detector is approaching its RC cutoff frequency, thus giving 1.4 dB smaller signal power than expected from theory. It is noted that this penalty can be compensated with more optical power input to the waveguide. Moreover, a larger frequency bandwidth can be achieved with the waveguide device. [10,11]
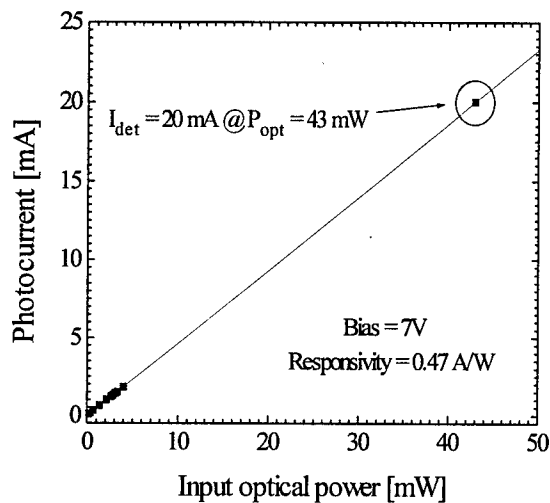


Fig. 7. DC photocurrent versus input optical power for the EA waveguide detector. A DC responsivity of 0.47 A/W is maintained up to 20 mA photocurrent.

Additionally, nonlinearity in the detector is observed at the second-harmonic frequency. The second-order intercept point (IP2) is extrapolated to +32.4 dBm (output referenced) from the measured second harmonics. This intercept point limits the dynamic range of the broadband link to approximately 98 dB for a 1 Hz noise bandwidth. Although the third harmonics are not detectable at the power levels used in this experiment, IP3 limits the single octave dynamic range of the link the same way as IP2 limits the multi-octave dynamic range. The conventional detector has an IP3 of +40 dBm.

In summary, a FKE electroabsorption waveguide transceiver device has been demonstrated to operate as a dual-function modulator and detector. The IP2 of the device operating as a detector is +32.4 dBm. The transceiver DC responsivity of 0.47 mA/mW causes a noise figure penalty of 4.7 dB compared to a conventional InGaAs detector.

14

## 5. Waveguide modulator based on combined FKE and QCSE

This program also studied a new method for achieving simultaneous second and third order nulls at one bias point in the transfer curve. As noted in Section 3, operating the modulator at the second order null maximizes the multi-octave SFDR and the link efficiency, while operating the modulator at the third order null has the benefit of maximum single-octave SFDR. In general, for both FKE and QCSE devices, the two null points occur at different bias voltages. However, due to their difference in behavior as a function of the detuned energy, it is possible to obtain a transfer curve that has overlapping second and third order null at the same bias voltage. A simulated transfer curve that possessed this characteristic is shown in Fig. 8.

Linearized modulator transfer curve
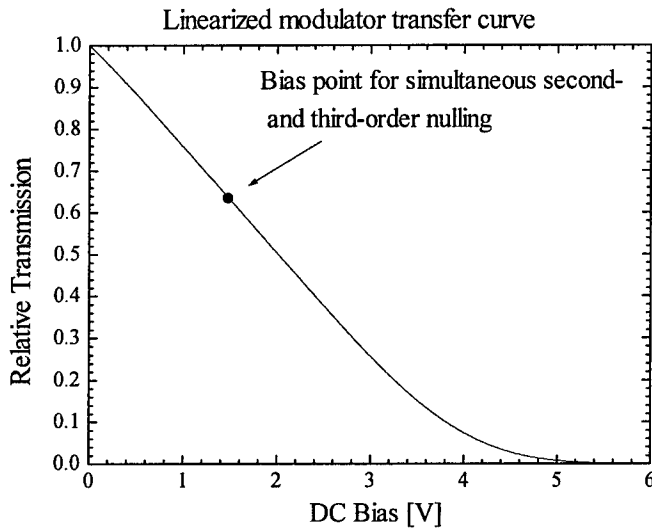
Fig. 8. A simulated transfer curve of an EA modulator that incorporates the FKE and QCSE in the same material structure.

A high linearity modulator has been designed based upon a combination of the FKE and QCSE in a single structure instead of two discrete modulators. The two are grown together in the same reactor, with one on top of the other on the same substrate. Thus they operate in parallel in the waveguide configuration. A computer code has been developed at UCSD to determine the layer parameters from the experimental transfer characteristics of the FKE and QCSE structures.

The strategy for achieving the linearized modulator relies on accurate models for the absorption coefficients of the two effects. The FKE absorption coefficient is modeled

after Tharmalingham [12] and the QCSE absorption coefficient is modeled after Chemla and Miller [13]. Additionally the modal distribution of light in the dielectric waveguide is calculated to give weighting to each absorption process. Finally, the transfer curve of the combination is generated and compared with that obtained from a grown structure.

Preliminary simulation results for both broadband and sub-octave links using the linearized electroabsorption modulator are shown in Fig. 9. Note that the coincidence of the second-order and third-order null points. The resultant link possesses a broadband SFDR of 121 dB-Hz$^{3/4}$ and a RF loss of 30 dB at 0.77 mA photocurrent.
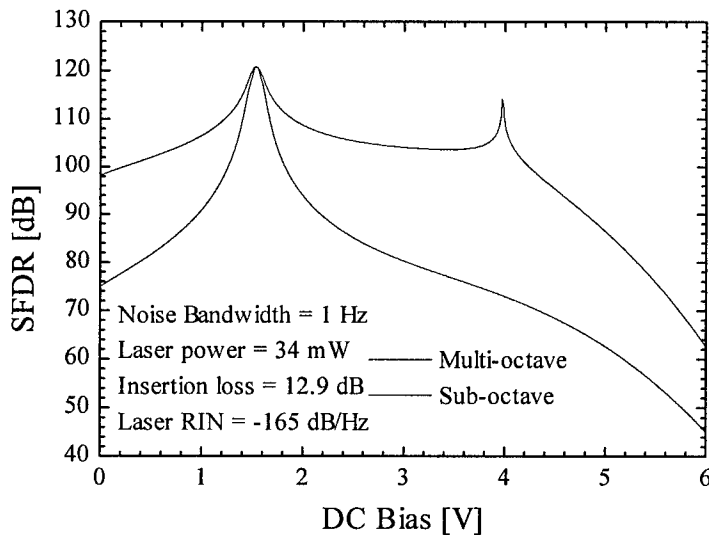


Fig. 9. Simulated SFDR of the waveguide modulator that incorporates the FKE and QCSE in the same material structure, the incident laser power is assumed to 30 mW and the second order and the third order nulls occur at the same bias.

In summary, a new concept has been conceived to achieve high linearity modulation in semiconductor electroabsorption waveguide modulators. This is based upon simultaneous nulling of the second and third derivative in the transfer curve using a combination of different electroabsorption effects. Simulation results show that a multi-octave SFDR of 121 dB-Hz$^{3/4}$ is possible with this approach.

# 6. Waveguide modulator based on longitudinal electric field effect in quantum wells

Conventional multiple quantum well (MQW) modulators are based on the transverse electric field quantum-confined Stark effect (QCSE). In this case, the electric field is applied perpendicular to the quantum wells. Excitons confined with the quantum well have strong transitions and sharp lineshape because of the localization of the electron and hole envelop functions. As the field increases, the exciton absorption peak is shifted to longer wavelengths due to the tilting of the energy bands of the quantum well, and reduces in strength due to the reduction of the overlap of the electron and hole envelop functions resulting from the tilt. The strong exitonic binding effect in quantum wells reduces the influence of thermal ionization, however, also results in strong wavelength dependence.

In this program, a different approach to the use of quantum well modulation is studied. Electroabsorption caused by exciton lifetime broadening was investigated. Consequently, the electric field is applied longitudinally to the quantum well layers. We call it a Longitudinal Electric field (LEF) modulator. Since the applied electric field is perpendicular to the direction of electron confinement, no tilting of the quantum well results. Any shift of the absorption edge is more like the Franz-Keldysh effect, and therefore is more gradual. On the other hand, the oscillator strength of the exciton is reduced upon the application of the longitudinal field, due to the change of the broadening of the exciton resonance. Since the reduction of the peak absorption is proportional to the applied field, the resultant intensity modulation is expected to be more linear than conventional QCSE modulators.

The experimental study explored the use of regrowth structures to enhance the passivation of the sidewall of the waveguide modulator for higher breakdown voltage, and at the same time, to place a lateral p-n junction for the quantum wells.

Epitaxial regrowth is one of the essential steps in the fabrication of a variety of devices and circuits in III-V semiconductor materials. Typically, prior to the regrowth, the semiconductor substrate is subject to a high temperature treatment (> 500 °C). This can lead to a deterioration of the exposed surfaces, thus compromising the device performance. By using a group V hydride over-pressure during the high temperature

heat-up or by using a reduced regrowth temperature, one can usually preserve the interface quality. However, for surfaces consisting of mixed group V elements, such as As and P, before the regrowth starts, an exchange reaction (e.g., As/P exchange) can occur in the presence of a group V ambient, resulting in a regrown interface with a composition-mixed transition region. This study employed in situ diffusion before regrowth in the MOVPE reactor to create a displacement of the pn junction away from the regrowth interface. This regrowth technique has also been employed in the fabrication of a transverse junction waveguide photodetector [see RL-TR-95-173]. It was shown that photodetectors made with in situ diffusion have better junction characteristics, such as a higher breakdown voltage and a lower leakage current, than those without [14]. The same technique is applied in the fabrication of the modulator to improve the regrown junction characteristics.

The materials used in this study are InP are InGaAs grown by low pressure MOVPE. The growth temperature and the chamber pressure are 650 °C and 20 Torr respectively for the first growth. Prior to the epitaxial regrowth, the exposed lateral surface of the mesa is placed under the partial pressure of phosphine and diethyl zinc at a lower temperature of 600 °C for the in situ diffusion.

The first growth for the waveguide modulator consists of three undoped lattice-matched layers (InP, InGaAs/InP MQWs, InP respectively), all 5000 Å thick, grown on a (100) oriented semi-insulating (SI) InP substrate. A 3-μm wide rib-waveguide is etched after the epitaxy using a non-selective etchant that stops in the lower cladding InP with a 1000 Å thick undoped InP layer left. This etchant is a solution of hydrogen peroxide, hydrogen bromine and water (1:1:40) which etches a non-reentrant sidewall profile on InP and InGaAs. A 1000 Å thick silicon dioxide is then deposited on the wafer using chemical vapor deposition and a 100 μm wide window is opened at one of the two sidewalls. After cleaning, the sample is reloaded into the MOVPE reactor. The unmasked surfaces are subject to the in situ zinc diffusion for 10 minutes at a temperature of 600 °C, at a diethyl zinc flow rate of 20 sccm and a phosphine flow rate of 120 sccm. After the diffusion, a 3000 Å thick p-type InP layer (at 5 sccm diethyl zinc) and a 1000 Å p+-InGaAs layer (at 17 sccm diethyl zinc) are grown right away. The total zinc diffusion distance is approximately 1 μm. Finally, AuZn/Au and AuGe/Au metal contacts are

fabricated at the p and n- regions by thermal evaporation. The substrate is lapped and mechanically cleaved into arrays of 250 μm long devices for evaluation. Fig. 10 shows the schematic cross section of the lateral junction waveguide MQW modulator after regrowth and metallization.



0.1 μm P⁺-InGaAs

AuZn / Au

InP (un.)

MQW (un.)

AuGe / Au

0.3 μm P-InP

InP (un.)

1 μm

Zn Diffused Region

SI InP
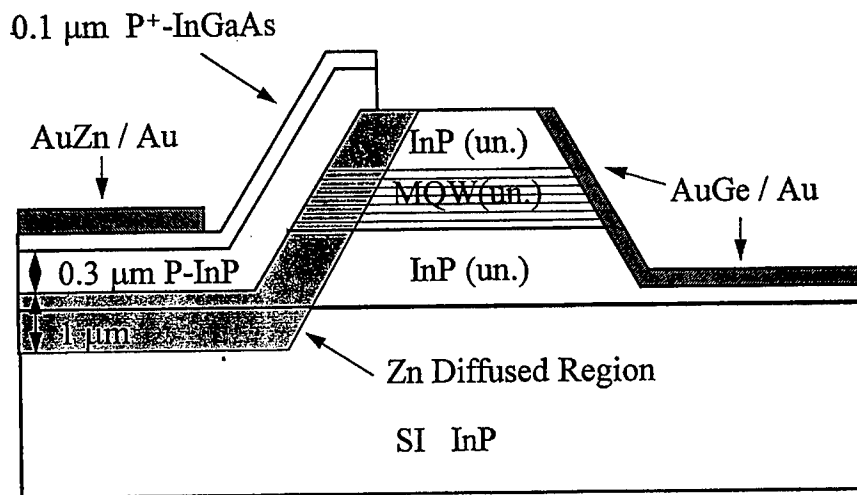
Fig. 10. Schematic cross-section view of the lateral junction waveguide MQW modulator.

The diodes showed a reverse breakdown voltage of larger than 30 V. The forward resistance is typically a few ohms for the above mentioned device dimensions. The measured capacitance is less than 0.05 pF when the reverse bias is larger than 5 V. This value is consistent with the capacitance calculated from the transverse junction dimensions. It implies a RC time constant of a few ps when the device is driven from a 50-Ω source. Fig. 11 and Fig. 12 show the typical transfer curve and modulation frequency response of the device, respectively. These results indicate that the 3 dB cutoff frequency of the device is not limited by the RC time effect at full depletion, but believed to be limited by the carrier transit time across the lateral depletion region.

Transverse Modulator #999
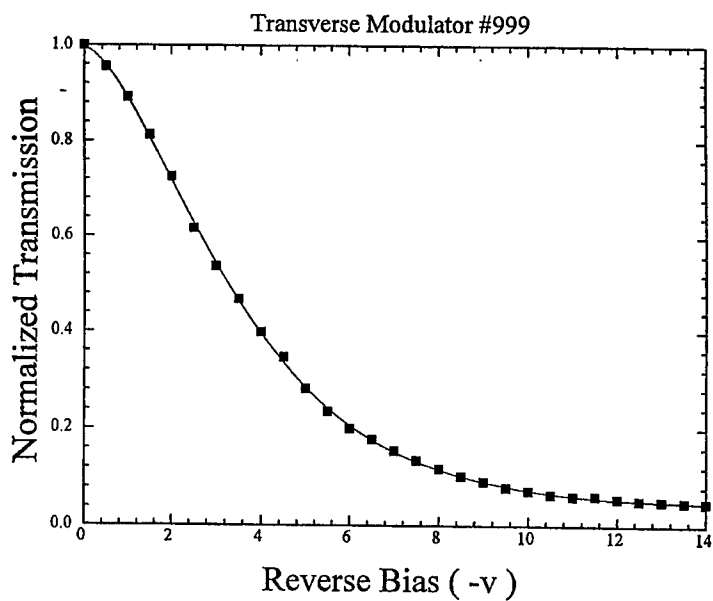
Fig. 11. Transfer curve characteristics of the lateral junction waveguide MQW modulator.
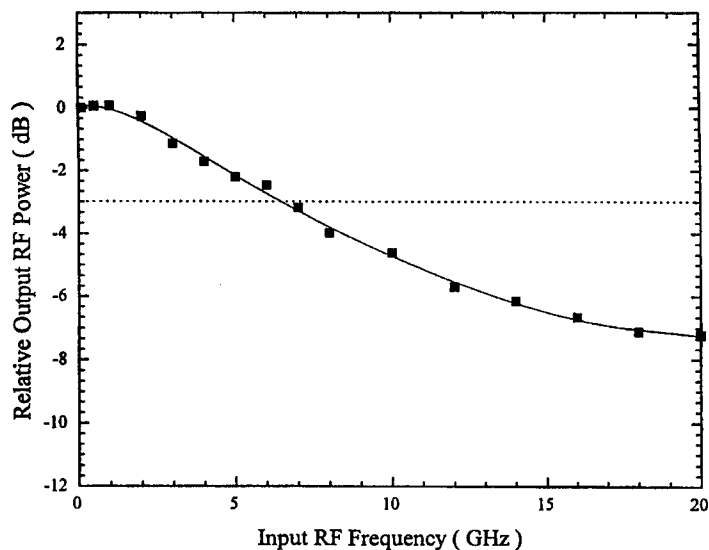
Fig. 12. The frequency response characteristics of the lateral junction waveguide MQW modulator at 1.5 μm wavelength.

In summary, a first time demonstration of a longitudinal electric field MQW modulator in InGaAs/InP MQWs has been accomplished. The modulation response is limited by the carrier transit time across the lateral depletion region in the multiple quantum well region.

# 7.   An experimental study of strained compensated InAsP/InGaP MQWs for waveguide modulator

Multiple quantum well (MQW) materials with bandgap around 0.8 - 0.95 eV ($\lambda$ = 1.3 - 1.55 $\mu$m) are of great importance because of their applications in optoelectronic devices for fiber-optic communication. Conventionally, the MQWs optoelectronic devices operating at 1.5 $\mu$m are limited to material systems lattice matched to InP, such as InGaAs(P)/InP or InGa(Al)As/InAlAs/InP. Recently, strained MQW structures have been used to improve the performance, such as polarization sensitivity of optoelectronic devices. For optical modulators a large number (> 10) of QWs can be used to provide an acceptable signal extinction ratio. Therefore it is desirable to reduce the net strain in the MQW structure.

Strained InAsP/InP MQW materials have been previously proposed as an alternative material system for optical devices. However, the net strain in one period of the InAsP/InP QW can place a limit to the maximum number of QWs that can be grown without dislocation. Unlike InAsP, InGaP is under tension when grown on InP. Thus, the compressive strain induced by the InAsP layer can be counteracted by growing InGaP barriers. Such a scheme has been employed in InAsP/InGaP MQWs at 1.06 $\mu$m grown by gas source MBE. In this program, we studied strain compensated InAsP/InGaP MQWs in the wavelength range of 1.3 - 1.5 $\mu$m where a larger strain needs to be balanced between the well and the barrier materials.

This program has demonstrated the successful growths of strain compensated InAs$_{0.66}$P$_{0.34}$ / InP /In$_{0.74}$Ga$_{0.26}$P MQWs at 1.3 and 1.5 $\mu$m by OMVPE. It is shown that, using a composite barrier structure, the net strain of the MQWs can be tuned around the zero strain point without affecting the operating wavelength.

The MQWs were grown in an infrared lamp-heated, horizontal low pressure MOVPE reactor. The substrate is (100) S-doped InP. The growth temperature and pressure were 550 °C (instead of 650) and 20 Torr respectively. The InAsP well layer is 54 Å thick. The barrier layer of the strained InAsP/InP MQWs consists of 140 Å of InP. In the strain compensated samples, the composite barrier region consists of an InGaP layer sandwiched between two InP layers. For these strain compensated QWs, the exciton

21

absorption peak is mainly determined by the InAsP well; the strain can be separately tuned by changing either the thickness or the composition of the InGaP layer, with the InP layer serving as a buffer. The composition of the InGaP layer is the same for the strain compensated samples with a Ga mole fraction of 0.26. To demonstrate the tuning of the net strain induced by such a barrier structure, the InGaP in the composite barrier in three of the samples were chosen to be 46, 72, and 101 Å, respectively. The thickness of the InP layers were adjusted accordingly to maintain the same barrier region thickness of 140 Å.
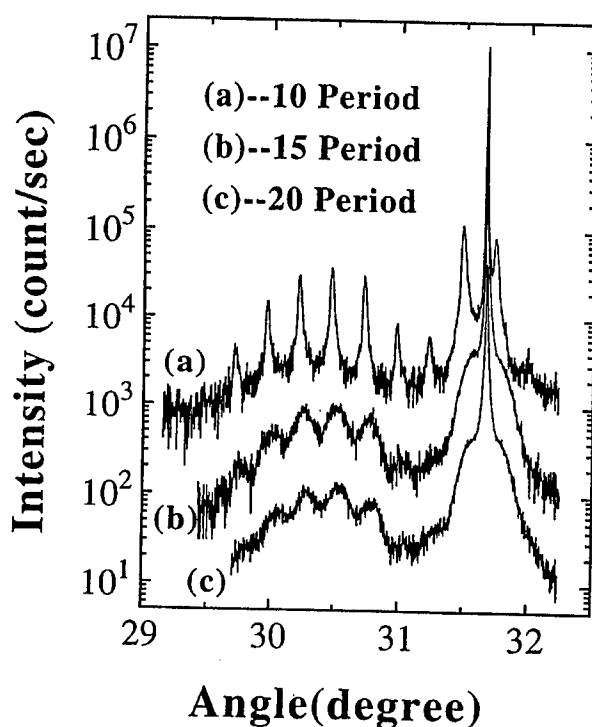


Fig. 13. X-ray rocking curves of 10, 15 and 20 period strained $InAs_{0.66}P_{0.34}$/InP MQWs samples grown under the same condition by OMVPE.

For the sake of comparison, the X-ray rocking curves of 10, 15, and 20 period strained $InAs_{0.66}P_{0.34}$ /InP ( $\lambda$=1.5 μm) MQW samples grown under similar condition are shown in Fig. 13. Sharp satellite peaks are observed in the X-ray rocking curve of the 10 period InAsP/InP MQWs. Due to the large compressive strain in the structure, the satellite peaks are higher at the lower angle side with respect to the substrate peak. In contrast to the 10 period sample, the 15 and 20 period InAsP/InP MQW samples show much broader satellite peaks. Cross hatches are unambiguously observed on these two samples under the microscope. These results suggest that the 15 and 20 period MQWs

are partially relaxed mainly due to the large net strain in the $InAs_{0.66}P_{0.34}$ /InP QWs. The corresponding low temperature photoluminescence (LTPL) spectra of the samples are shown in Fig. 14. The shift of the luminescence peak of the 20 period sample is consistent with the strain relaxation. It is noteworthy that the LTPL spectra of the 10 and 15 period samples are similar and they have the same full width at half maximum (FWHM) of 25 meV while there is a substantial difference between their X-ray rocking curves. The relatively large FWHM of the LTPL suggests that there may be some partial relaxation in the 10 period sample even though it has good X-ray diffraction features and good surface morphology.

The X-ray rocking curves and LTPL spectra of InAsP/InP/InGaP/InP strain compensated MQW samples with different InGaP thickness are shown in Fig. 15 and Fig. 16 respectively. Very sharp satellite peaks in the X-ray rocking curves were observed in all three samples.
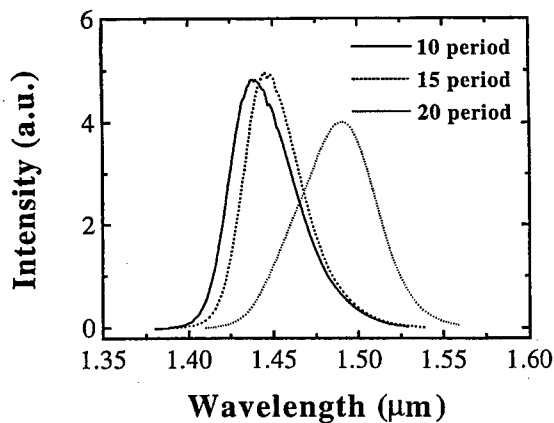
Fig. 14. Low temperature photoluminescence spectra of the period strained $InAs_{0.66}P_{0.34}$/InP MQWs samples shown in Fig. 13.
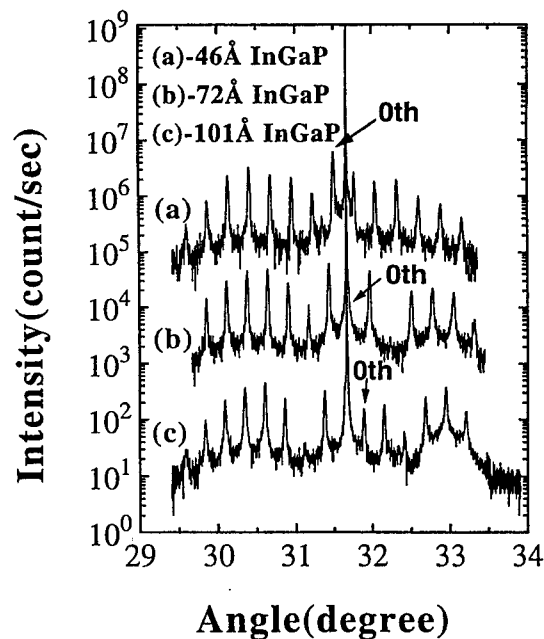
Fig. 15. X-ray rocking curves of strained compensated $InAs_{0.66}P_{0.34}$/InP/ $In_{0.74}Ga_{0.26}P$ MQWs samples with InGaP thicknesses of 46 Å, 72 Å and 101 Å respectively.

Fig. 15 shows that the zeroeth order satellite peak of the MQWs can be shifted from the smaller angle side to the larger angle side with respect to the substrate peak by varying the InGaP thickness. The net strain in the MQWs structure changes from 0.24% (compressive) to -0.27% (tensile). For the 72 Å InGaP sample, a very small net strain is obtained. Strong photoluminescence was also obtained from all of the strain compensated MQW samples. The FWHMs measured from Fig. 16 are around 14 meV, which are much improved over those of the uncompensated MQWs shown in Fig. 14.
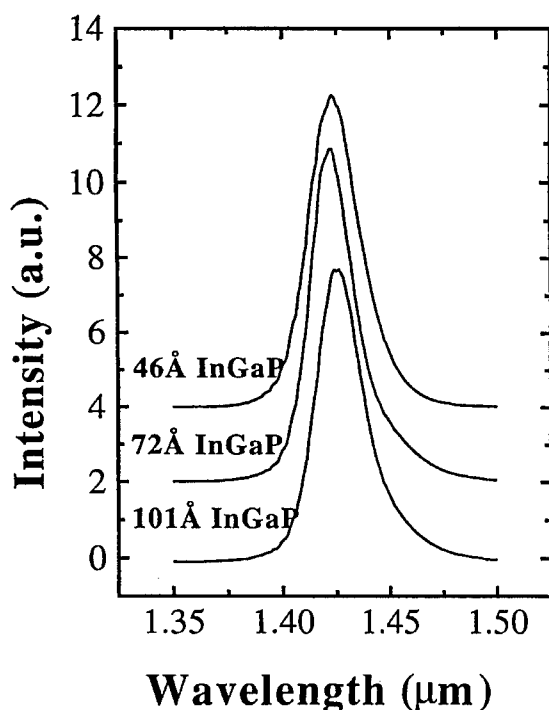


Fig. 16. Low temperature photoluminescence spectra of $InAs_{0.66}P_{0.34}$/InP/ $In_{0.74}Ga_{0.26}P$ MQWs samples shown in Fig. 15.
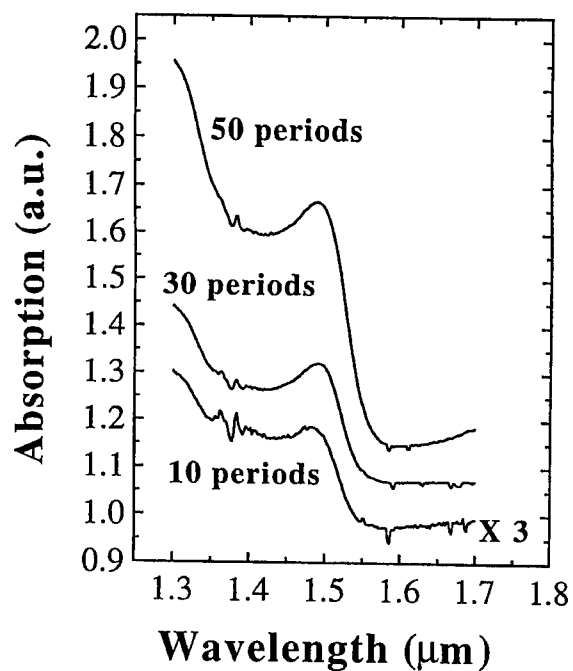
Fig. 17. Room temperature optical absorption spectra of 10, 30 and 50 period strain compensated $InAs_{0.66}P_{0.34}$/InP/ $In_{0.74}Ga_{0.26}P$ MQWs samples with 72 Å thick InGaP in the composite barrier. The spectrum for the 10 period one has been multiplied by a factor of 3.

With this InP/InGaP/InP sandwiched barrier, the peak photoluminescence wavelength of the strain compensated MQWs changes very little ( < 10 Å) as the strain undergoes a total change of 0.51%. With a closely strain compensated MQW structure, in principle a large number of periods can be grown with good quality. To demonstrate this, strain compensated MQW samples with 30 and 50 periods with 72 Å InGaP were grown.

Again both samples exhibit sharp satellite peaks in the X-ray rocking curves. Fig. 17 compares the room temperature optical absorption spectra of 10, 30 and 50 period MQWs samples. No deterioration of the exciton absorption peak is observed and they have the same half width of half maximum of 18 meV.

In summary, good quality strain compensated $InAs_{0.66}P_{0.34}/InP/In_{0.74}Ga_{0.26}P$ MQWs for 1.3 - 1.5 $\mu$m wavelength have been grown by MOVPE and their X-ray rocking curves and photoluminescence spectra compared with those of strained $InAs_{0.66}P_{0.34}$ /InP MQWs. With the composite InP/InGaP/InP barrier structure, the net strain of the MQWs can be successfully tuned without affecting the operating wavelength. Finally, thick (up to 50 periods, 1 $\mu$m total thickness) strain compensated MQWs were grown and no deterioration of either crystalline and optical properties has been observed. The next step is to investigate these materials for waveguide modulator applications.

## 8. Conclusion and Future Plans

Within the duration of this program, we have demonstrated much exciting progress towards the use of semiconductor waveguide modulator for analog fiber optic applications. We demonstrated that the FKE waveguide modulator can compete well with those made of lithium niobate materials in meeting the analog RF link requirements. We have also shown the small size of the semiconductor device can be useful for the size reduction at the transmitter, and for the dual use of the semiconductor waveguide as modulator and detector.

We have also started the work on a material structure that combined both FKE and QCSE for modulation. More experimental works on this topic will be reported in the near future.

In the area of quantum well devices, we have demonstrated longitudinal electric field can be used in the quantum well for effective modulation, though future designs should emphasize the modification for high frequency operation. The use of the strain-compensated materials for modulation proved to be a viable concept as high optical quality materials can be readily grown.

There are other practical issues that needed to be addressed in future programs on semiconductor electroabsorption waveguide modulators, namely, the reduction of optical insertion loss so that it is comparable to those of lithium niobate devices; the reduction of temperature and polarization sensitivity; also, maintaining high performance up to high frequency operation. Finally, the package and reliability studies of the semiconductor electroabsorption device will be essential for practical applications.

## References

1. S. Korotky, R. De Ridder, "Dual Parallel Modulation Schemes for Low-Distortion Analog Optical Transmission," *IEEE J. on Selected Areas in Commun.*, Vol. 8, No. 7, pp. 1377-1381, 1990.

2. L. Johnson, H. Rousell, "Linearization of an Interferometric Modulator at Microwave Frequencies by Polarization Mixing," *IEEE Photon. Technol. Lett.*, Vol. 2, No. 11, pp. 810-811, 1990.

3. L. Fock, R. Turner, "Reduction of Distortion in Analogue Modulated Semiconductor Lasers by Feedforward Compensation," *Electron. Lett.*, Vol. 27, No. 8, pp. 669-671, 1991.

4. W.B. Yu, "A Linearized Optical Modulator for Reducing Third-Order Intermodulation Distortion," *IEEE J. of Lightwave Technol.*, Vol. 10, No. 8, pp. 1066-1070, 1992.

5. W. Franz, *Z. Naturforsch.*, Vol. 13a, p. 484, and L. Keldysh, *Soviet J. of Physics JETP*, Vol. 7, p. 788, 1958.

6. B. Knüpfer, P. Kiesel, M. Kneissl, S. Dankowski, N. Linder, G. Weimann, G.H. Döhler, "Polarization-Insensitive High-Contrast GaAs/AlGaAs Waveguide Modulator Based on the Franz-Keldysh Effect," *IEEE Photon. Technol. Lett.*, Vol. 5, No. 12, pp. 1386-1388, 1993.

7. G. Mak, C. Rolland, K. Fox, C. Blaauw, "High-Speed Bulk InGaAsP-InP Electroabsorption Modulators with Bandwidth in Excess of 20 GHz," *IEEE Photon. Technol. Lett.*, Vol. 2, No. 10, pp. 730-733, 1990.

8. G. Betts, L. Walpita, W. Chang, R. Mathis, "On the Linear Dynamic Range of Integrated Electrooptical Modulators," *IEEE J. of Quantum Electron.*, Vol. QE-22, No. 7, pp. 1009-1011, 1986.

9. G. Giuliani, P. Cinguino, V. Seano, "Multifunctional characteristics of 1.5 mm two-section amplifier-modulator-detector SOA," IEEE Photon. Technol. Lett., Vol. 8, No. 3, pp. 367-369, 1996.

10. A.R. Williams, A.L. Kellner, P.K. L. Yu, "High frequency saturation measurements of an InGaAs/InP waveguide photodetector," Electronics Lett., Vol 29, No. 14, pp. 1298-1299, 1993.

11. M.C. Wu, L.Y. Lin, T. Itoh, "A new ultrafast photodetector : optical-to-microwave transformer," Proc. SPIE, Generation, Amplification, and Measurement of Ultrashort Laser Pulses, Vol. 2116, pp. 228-236, 1994.

12. K. Tharmalingam, "Optical Absorption in the presence of a Uniform Field," Physics Review, Vol., 130, No. 6, pp. 2204-2206, 1963.

13. D.S. Chemla, D.A. B. Miller, "Room-temperature exciton nonlinear-optical effects in semiconductor quantum-well structures," J. Opt. Soc. Am. B, Vol. 2, No. 7, pp. 1155-1173, 1985.

14. D.P. Luo, J.T. Zhu, A. L. Kellner, and P.K.L. Yu, "Transverse Junction Waveguide InGaAs/InP Photodiodes," IEE Electronics Lett., Vol. 31, 1872-1873, 1995

## 9. List of publications sponsored by this contract

1. A.R. Clawson, X. Jiang, P.K.L. Yu, C.M. Hanson and T.T. Vu, "Interface Strain in OMVPE Grown InGaAs/InP Superlattices," *J. Electronics Materials* , Vol. 22, p. 155-160 (1993).

2. P.K.L. Yu, M. Markarian, R. Welstand, X.S. Jiang, A.R. Clawson, and S.S. Lau, "Strained InAsP/InGAP MQWs Grown by MOVPE,". SPIE Conference proceedings on Technologies for Optical Fiber Comminications, Vol. 2149, 44-53 (1994).

3. Y.Z. Liu, J.M. Chen, S.A. Pappert, R.J. Orazo, A.R. Williams, A.L. Kellner, X.S. Jiang, and P.K.L. Yu, "Semiconductor electroabsorption waveguide modulator for shipboard analog link applications," SPIE proceedings on Optoelectronic Signal Processsing for Phased-Array Antennas IV, Vol 2155, 98-106 (1994).

4. X.S. Jiang, A.R. Clawson, and P.K.L. Yu, "InP-on-InGaAs Interface with Ga and In Coverage in MOVPE of InGaAs/InP Superlattices," *J. Crystal Growth* , Vol. 147, p. 8-12 (1995).

5. X.S. Jiang and P.K.L. Yu, "Strain compensated InAsP/InP/InGaP MQWs at 1.5 µm Wavelength," *Appl. Phys. Lett.,* Vol. 65, p. 2536-2538 (1995).

6. S.A. Pappert, C.K. Sun, and R. J. Orazi, R.B. Welstand, and P.K.L. Yu, "Performance Comparison of Mach-Zehnder and Electroabsorption Modulators for Analog Photonic Links," *Proceeding of Photonic Systems for Antenna Applications* PSAA-5, p. 123-128 (1995).

7. C.K. Sun, S.A. Pappert, R.B. Welstand, J.T. Zhu, P.K.L. Yu, Y.Z. Liu, and J.M. Chen, "High Spurious Free Dynamic Range Fiber Link Using A Semiconductor Electroabsorption Modulator," *Electronics Lett.,* Vol. 31, p. 902-903 (1995).

8. S.A. Pappert, C.K. Sun, R.B. Welstand, P.K.L. Yu, Y. Z. Liu, and J.M. Chen, "High Dynamic Range Fiber Optic Links Using Semiconductor Electroabsorption Modulator", Proceeding of IEEE LEO Summer Meeting on RF Optoelectronics, Keystone, Colorado, Aug, 1995.

9. R.B. Welstand, C.K. Sun, S. A. Pappert, Y.Z. Liu, J.M. Chen, J.T. Zhu, A.L. Kellner, P.K.L. Yu, "Enhanced Linear Dynamic Range property of Franz-Keldysh

Effect Waveguide Modulator," *IEEE Photonics Technology Lett*, Vol. 7, p. 751-753 (1995).

10. R.B.Welstand, C.K. Sun, Y.Z. Liu, S. A. Pappert, J.T. Zhu, J.M. Chen, P.K.L. Yu, "High dynamic range in electroabsorption modulator for analog links," Proc. of SPIE, Vol. 2560, pp. 44-49 (1995).

11. J.T. Zhu, A.R. Clawson, and P.K.L. Yu, "High Quality $In_{1-x}(Ga_x)As_yP_{1-y}/InP$ compressive Strain Quantum Well Structures Grown by LP-MOCVD," *Proc. of Mat. Res. Soc.*, pp. 45-50 (1996).

12. R.B. Welstand, C.K. Sun, S.A. Pappert, Y.Z. Liu, Q.Z. Liu, S.S. Lau and P.K.L. Yu, "High Dynamic Range Fiber-optic Links using III-V Electroabsorption Modulators," Proceeding of PSAA-6, the sixth annual ARPA Symposium on Photonic Systems for Antenna Applications, Mar 5-7, 1996, Monterey, CA.

13. R.B. Welstand, C.K. Sun, S.A. Pappert, Y.Z. Liu, P.K.L. Yu, "High Dynamic Range Semiconductor Electroabsorption Modulator Structures," Proceeding of The 5th Biennial Department of Defense Photonics Conference, p. 209-212, March 26-28, 1996. McLean, Virginia

14. R.B. Welstand, S.A. Pappert, C.K. Sun, J.T. Zhu, Y.Z. Liu, P.K.L. Yu, "Dual-Function Electroabsorption Waveguide Modulator/Detector for Optoelectronic Transceiver Applications," IEEE *Photonics Technical Letters*, 8, p. 1540-1542, (1996).

15. R.B. Welstand, R. J. Orazi, C.K. Sun, H. G. Rao, Y.Z. Liu, S.A. Pappert, and P.K.L. Yu, "Phase Noise and Dynamic Range of Analog Fiber Links using Electroabsorption Modulators", Proceeding the SPIE Symposium, Vol. 2844, pp. 34-39 (1996).

## 10. List of presentations sponsored by this contract

1. P.K.L. Yu, M. Markarian, R. Welstand, X.S. Jiang, A.R. Clawson, and S.S. Lau, "Strained InAsP/InGaP MQWs Grown by MOVPE,". SPIE Conference on Technologies for Optical Fiber Comminications, Los Angeles, CA., January 1994.

2. Y.Z. Liu, J.M. Chen, S.A. Pappert, R.J. Orazi, A.R. Williams, A.L. Kellner, X.S. Jiang, and P.K.L. Yu, "Semiconductor electroabsorption waveguide modulator for shipboard analog link applications," SPIE Conference on Optoelectronic Signal Processsing for Phased-Array Antennas IV, Los Angeles, CA., January 1994.

3. P.K.L. Yu and A.L. Kellner, "High Linearity Modulation in Quantum Wells for Analog Fiber Optic Links", ARPA/MTO Optics Reviews, Monterey CA., June 1994

4. X.S. Jiang, R.B. Welstand, M. Markarian, C.A. Clawson, S.S. Lau, and P.K.L. Yu, "Strained InAsP/InGaP Superlattice Grown by MOVPE", The 36th Electronic Material Conference at Boulder, Colorado, June 1994.

5. S.A. Pappert, C.K. Sun, and R.J. Orazi, R.B. Welstand, and P.K.L. Yu, "Performance Comparison of Mach-Zehnder and Electroabsorption Modulators for Analog Photonic Links," *Photonic Systems for Antenna Applications* PSAA-5, Monterey, CA., January, 1995.

6. R.B. Welstand, C.K. Sun, Y.Z. Liu, S. A. Pappert, J.T. Zhu, J.M. Chen, P.K.L. Yu, "High dynamic range in electroabsorption modulator for analog links," SPIE Symposium, San Diego, CA., July 1995.

7. P.K.L. Yu and A.L. Kellner, "High Linearity Modulation in Quantum Wells for Analog Fiber Optic Links", ARPA/MTO Optics Review, Big Sky, Montana, July 1995.

8. S.A. Pappert, C.K. Sun, R.B. Welstand, P.K.L. Yu, Y.Z. Liu, and J.M. Chen, "High Dynamic Range Fiber Optic Links Using Semiconductor Electroabsorption Modulator", IEEE LEO Summer Meeting on RF Optoelectronics, Keystone, Colorado, Aug, 1995.

9. J.T. Zhu, A.R. Clawson, and P.K.L. Yu, "High Quality $In_{1-x}(Ga_x)As_yP_{1-y}/InP$ compressive Strain Quantum Well Structures Grown by LP-MOCVD," *Symposium of Mat. Res. Soc.,* San Francisco, CA., April 1996.

31

10. R.B. Welstand, C.K. Sun, S.A. Pappert, Y.Z. Liu, Q.Z. Liu, S.S. Lau and P.K.L. Yu, "High Dynamic Range Fiber-optic Links using III-V Electroabsorption Modulators," Proceeding of PSAA-6, the sixth annual ARPA Symposium on Photonic Systems for Antenna Applications, Mar 5-7, 1996, Monterey, CA.

11. R.B. Welstand, C.K. Sun, S.A. Pappert, Y.Z. Liu, P.K.L. Yu, "High Dynamic Range Semiconductor Electroabsorption Modulator Structures," The 5th Biennial Department of Defense Photonics Conference, March 26-28, 1996. McLean, Virginia

12. R.B. Welstand, R.J. Orazi, C. K. Sun, H.G. Rao, Y.Z. Liu, S. A. Pappert, and P.K.L. Yu, "Phase Noise and Dynamic Range of Analog Fiber Links using Electroabsorption Modulators", SPIE Symposium at Denver, Co., August 1996.

13. P.K.L. Yu, "Semiconductor Waveguide Components for Analog Fiber-Optics Links", presented at the WRI International Symposium, Polytechnic University, Brooklyn, NY. September 10-12, 1996.

14. P.K.L. Yu , "Semiconductor Waveguide Modulators and Detectors for Analog Fiber-Optic Links", presented at Rome Laboratory on September 19, 1996.

## 11. List of Ph.D. dissertations related to this contract

1. "Growth of InGaAs/InP Multiple Quantum Well by Metalorganic Vapor Phase Epitaxy," by Xiao Song Jiang, UCSD, 1994.

2. "High linearity modulation and detection in semiconductor electroabsorption waveguides" by Robert B. Welstand, UCSD, in preparation.

# DISTRIBUTION LIST

| addresses | number of copies |
|---|---|
| JAMES R. HUNTER<br>ROME LABORATORY/OCPC<br>25 ELECTRONIC PKY<br>ROME NY 13441-4515 | 10 |
| UNIV OF CALIFORNIA, SAN DIEGO<br>DEPT OF ELECTRICAL & COMPUTER ENG<br>LAJOLLA CA  92093-0407 | 5 |
| ROME LABORATORY/SUL<br>TECHNICAL LIBRARY<br>26 ELECTRONIC PKY<br>ROME NY 13441-4514 | 1 |
| ATTENTION:  DTIC-OCC<br>DEFENSE TECHNICAL INFO CENTER<br>8725 JOHN J. KINGMAN ROAD, STE 0944<br>FT. BELVOIR, VA 22060-6218 | 2 |
| ADVANCED RESEARCH PROJECTS AGENCY<br>3701 NORTH FAIRFAX DRIVE<br>ARLINGTON VA 22203-1714 | 1 |
| RELIABILITY ANALYSIS CENTER<br>201 MILL ST.<br>ROME NY 13440-8200 | 1 |
| ATTN:  RAYMOND TADROS<br>GIDEP<br>P.O. BOX 8000<br>CORONA CA 91718-8000 | 1 |

```
AFIT ACADEMIC LIBRARY/LDEE                          1
2950 P STREET
AREA B, BLDG 642
WRIGHT-PATTERSON AFB OH 45433-7765


ATTN:  R.L. DENISON                                 1
WRIGHT LABORATORY/MLPO, BLDG. 651
3005 P STREET, STE 6
WRIGHT-PATTERSON AFB OH 45433-7707


WRIGHT LABORATORY/MTM, BLDG 653                      1
2977 P STREET, STE 6
WRIGHT-PATTERSON AFB OH 45433-7739


WRIGHT LABORATORY/FIVS/SURVIAC                       1
2130 EIGHTH STREET, BLDG 45, STE 1
WRIGHT-PATTERSON AFB OH 45433-7542


ATTN:  GILBERT G. KUPERMAN                           1
AL/CFHI, BLDG. 248
2255 H STREET
WRIGHT-PATTERSON AFB OH 45433-7022


OL AL HSC/HRG, BLDG. 190                             1
2698 G STREET
WRIGHT-PATTERSON AFB OH 45433-7604


AUL/LSAD                                            1
600 CHENNAULT CIRCLE, BLDG. 1405
MAXWELL AFB AL 36112-6424


US ARMY STRATEGIC DEFENSE COMMAND                   1
CSSD-IM-PA
P.O. BOX 1500
HUNTSVILLE AL 35807-3801
```

```
COMMANDING OFFICER                                          1
NCCOSC RDT&E DIVISION
ATTN: TECHNICAL LIBRARY,CODE 0274
53560 HULL STREET
SAN DIEGO CA 92152-5001

COMMANDER, TECHNICAL LIBRARY                               1
4747000/C0223
NAVAIRWARCENWPNDIV
1 ADMINISTRATION CIRCLE
CHINA LAKE CA 93555-6001


                                                           2
SPACE & NAVAL WARFARE SYSTEMS CMD
ATTN:  PMW163-1 (R. SKIANO) OT-1 ROOM 1044A
53560 HULL ST.
SAN DIEGO, CA 92152-5002


SPACE & NAVAL WARFARE SYSTEMS                              1
COMMAND, EXECUTIVE DIRECTOR (PD13A)
ATTN:  MR. CARL ANDRIANI
2451 CRYSTAL DRIVE
ARLINGTON VA 22245-5200

COMMANDER, SPACE & NAVAL WARFARE                           1
SYSTEMS COMMAND (CODE 32)
2451 CRYSTAL DRIVE
ARLINGTON VA 22245-5200


CDR, US ARMY MISSILE COMMAND                               2
RSIC, BLDG. 4484
AMSMI-RD-CS-R, DOCS
REDSTONE ARSENAL AL 35898-5241


ADVISORY GROUP ON ELECTRON DEVICES                         1
SUITE 500
1745 JEFFERSON DAVIS HIGHWAY
ARLINGTON VA 22202


REPORT COLLECTION, CIC-14                                  1
MS P364
LOS ALAMOS NATIONAL LABORATORY
LOS ALAMOS NM 87545


AEDC LIBRARY                                               1
TECHNICAL REPORTS FILE
100 KINDEL DRIVE, SUITE C211
ARNOLD AFB TN 37389-3211
```

```
COMMANDER                                          1
USAISC
ASHC-IMD-L, BLDG 61801
FT HUACHUCA AZ 85613-5000


US DEPT OF TRANSPORTATION LIBRARY                  1
FB10A, M-457, RM 930
800 INDEPENDENCE AVE, SW
WASH DC 22591


AFIWC/MSO                                          1
102 HALL BLVD, STE 315
SAN ANTONIO TX 78243-7016


NSA/CSS                                            1
K1
FT MEADE MD 20755-6000


PHILLIPS LABORATORY                                1
PL/TL (LIBRARY)
5 WRIGHT STREET
HANSCOM AFB MA 01731-3004


THE MITRE CORPORATION                              1
ATTN: E. LADURE
D460
202 BURLINGTON RD
BEDFORD MA 01732

OUSD(P)/OTSA/DUTD                                  2
ATTN:   PATRICK G. SULLIVAN, JR.
400 ARMY NAVY DRIVE
SUITE 300
ARLINGTON VA 22202

ROME LABORATORY/ERO                                1
ATTN:   RICHARD PAYNE
HANSCOM AFB, MA   01731-5000


ROME LABORATORY/EROC                               1
ATTN:   JOSEPH P. LORENZO, JR.
HANSCOM AFB, MA   01731-5000
```

```
ROME LABORATORY/EROP                                    1
ATTN:   JOSEPH L. HORNER
HANSCOM AFB, MA   01731-5000


ROME LABORATORY/EROC                                    1
ATTN:   RICHARD A. SOREF
HANSCOM AFB, MA   01731-5000


ROME LABORATORY/ERXE                                    1
ATTN:   JOHN J. LARKIN
HANSCOM AFB, MA   01731-5000


ROME LABORATORY/ERDR                                    1
ATTN:   DANIEL J. BURNS
525 BROOKS RD
ROME NY   13441-4505


ROME LABORATORY/IRAP                                    1
ATTN:   ALBERT A. JAMBERDINO
32 HANGAR RD
ROME NY   13441-4114


ROME LABORATORY/OCP                                     1
ATTN:   BRIAN M. HENDRICKSON
25 ELECTRONIC PKY
ROME NY   13441-4515


ROME LABORATORY/C3BC                                    1
ATTN:   ROBERT L. KAMINSKI
525 BROOKS RD
ROME NY   13441-4505


ROME LABORATORY/OCP                                     1
ATTN:   MAJOR GARY D. BARMORE
25 ELECTRONIC PKY
ROME NY   13441-4515


ROME LABORATORY/OCP                                     1
ATTN:   JOANNE L. ROSSI
25 ELECTRONIC PKY
ROME NY   13441-4515
```

NY PHOTONIC DEVELOPMENT CORP          1
MVCC ROME CAMPUS
UPPER FLOYD AVE
ROME, NY   13440

# MISSION
## OF
# ROME LABORATORY

Mission. The mission of Rome Laboratory is to advance the science and technologies of command, control, communications and intelligence and to transition them into systems to meet customer needs. To achieve this, Rome Lab:


   a. Conducts vigorous research, development and test programs in all applicable technologies;

   b. Transitions technology to current and future systems to improve operational capability, readiness, and supportability;

   c. Provides a full range of technical support to Air Force Material Command product centers and other Air Force organizations;

   d. Promotes transfer of technology to the private sector;

   e. Maintains leading edge technological expertise in the areas of surveillance, communications, command and control, intelligence, reliability science, electro-magnetic technology, photonics, signal processing, and computational science.


The thrust areas of technical competence include: Surveillance, Communications, Command and Control, Intelligence, Signal Processing, Computer Science and Technology, Electromagnetic Technology, Photonics and Reliability Sciences.